

Supporting Information

Abnormally inhibiting effect of H₂O on Pd/SiO₂ and Na-Pd/SiO₂ catalysts for HCHO oxidation

Chunying Wang^{a, b}, Jingyi Wang^{a, b}, Xiaofeng Liu^a, Yaobin Li^{a, b, *}, Changbin Zhang^c,
Yuming Zheng^a, Wenpo Shan^{a, b, *}

^a Center for Excellence in Regional Atmospheric Environment, Key Laboratory of Urban Pollutant Conversion, Institute of Urban Environment, Chinese Academy of Sciences, Xiamen 361021, China.

^b Zhejiang Key Laboratory of Urban Environmental Processes and Pollution Control, **CAS Haixi Industrial Technology Innovation Center in Beilun, Ningbo 315800, China.**

^c State Key Joint Laboratory of Environment Simulation and Pollution Control, Research Center for Eco-environmental Sciences, Chinese Academy of Sciences, Beijing, 100085, China.

* Corresponding Authors:

Email: ybli@iue.ac.cn (Y. Li), wpshan@iue.ac.cn (W. Shan)

Catalyst characterization

The X-ray powder diffraction (XRD) patterns of the catalysts were obtained using a wide-angle X'Pert Pro XRD diffractometer (PANalytical B.V., Netherlands). The measurements were conducted with Cu K α radiation ($\lambda=1.5406$ Å) at 40 kV and 40 mA, with a scanning speed of 2 °/min. The diffraction patterns were collected in the 2θ range of 5° to 90°.

High-angle annular dark-field scanning transmission electron microscopy (HAADF-STEM) was performed using a JEOL JEM-ARM2100F TEM equipped with a Cs-corrected probe. The instrument operated at 200 kV.

To characterize the specific surface area and pore properties of the catalysts, nitrogen (N₂) physisorption was carried out at -196 °C using a Quantachrome Quadrasorb SI-MP analyzer. Prior to the physisorption measurement, the catalysts were degassed at 300 °C for 1 hour. The specific surface areas were calculated from the isotherms by applying the BET equation in the partial pressure range of 0.05-0.3. CO chemisorption was analyzed using a dynamic pulse method.^{1,2}

Electron spin-resonance spectroscopy (ESR) spectra were collected using a Benchtop Micro-ESRTM machine (Active Spectrum, Inc.) at a microwave frequency of 9.70 GHz and a temperature of 90 K. The ESR spectra were obtained without light irradiation.

HCHO oxidation, CO and NH₃ in-situ adsorption DRIFTS spectra were collected on a Thermo Fisher IS 50 spectrometer equipped with an MCT detector at room temperature. The catalyst needs to be pre-reduced before testing with H₂ at 350 °C for 1 h, followed by purging with He for 30 min, and followed by cooling down to 25 °C.

All spectra were measured at room temperature, with a resolution of 4 cm⁻¹ and accumulation of 100 scans.

X-ray photoelectron spectra (XPS) were measured by an X-ray source (ESCALAB 250 Xi, Thermo Fisher Scientific, USA) equipped with Al K α radiation (h ν = 1486.6 eV). The C 1s peak (284.8 eV) was used to calibrate the binding energy (BE) values.

The static water contact angle (CA) over laminated catalyst powders was determined on a contact angle meter (OCA 20, Dataphysics, Germany) in an environmental chamber saturated with water vapor under ambient conditions.

H₂O-TPD was performed on a Micromeritics AutoChem II 2920 apparatus. Firstly, the catalysts were reduced in situ with 10 vol. % H₂/Ar flow at 623 K for 1 h, then cooled down to 25 °C by purging with He. After that the system was switched to Loop, and performed 20 times water vapor pulse, then purged with He for 30 min. Subsequently, the carrier gas was switched to He for 20 min and the baseline was allowed to stabilize. Finally, the TCD signal in the temperature range 25-900 °C was recorded.

Activity test for HCHO oxidation

For HCHO activity evaluation, the inlet and outlet gases were monitored according to our previous work ³. In all the experiments, HCHO conversion was calculated using the following equation:

$$HCHO \text{ Conversion}(\%) = \left(1 - \frac{[HCHO]_{out}}{[HCHO]_{in}}\right) \times 100\%$$

The CO₂ yield was defined as follows:

$$CO_2 \text{ Yield}(\%) = \frac{[CO_2]}{[HCHO]_{in}} \times 100\%$$

where [HCHO]_{in} and [HCHO]_{out} are the inlet and outlet HCHO concentrations, respectively. [CO₂] is the outlet CO₂ concentration, where [HCHO]_{in} and [HCHO]_{out} are the inlet and outlet HCHO concentrations, respectively.

The turnover frequency (TOF) at 25 °C was determined based on a separate experiment conducted to maintain the apparent conversion of HCHO below 20 %. This was achieved by adjusting the inlet HCHO concentration and the weight hourly space velocity (WHSV), while ensuring negligible heat and mass-transfer effects. TOF can be calculated using the following equation:

$$TOF = \frac{n_{HCHO}}{n_{Pd}} = \frac{[HCHO]_{in} \times \gamma \times V/R_g}{m_{cat.} \times \omega_{Pd} \times D_{Pd}/M_{Pd}}$$

Where the parameters are the molar weight of consumed HCHO per second (n'_{HCHO} , mol s⁻¹), molar weight of Pd exposed on TiO₂ surface (n'_{Pd} , mol), initial inlet concentration of HCHO ([HCHO]_{in}, ppm), total flow rate (V, Ls⁻¹), molar volume of gas at 25 °C and 101 kPa (R_g, 24.5 L mol⁻¹), weight of catalyst (m_{cat.}, g), loading percentage of Pd (ω_{Pd}, %), Pd dispersion (D_{Pd}, %) and molecular mass of Pd (M_{Pd}, gmol⁻¹), respectively.

Table S1 Comparison of the effect of water on the HCHO oxidation performance of different catalysts

Catalysts	Reaction conditions	HCHO conversion		Ref.
		Without H ₂ O	With H ₂ O	
Pd/TiO ₂	20 ppm HCHO, WHSV 200,000 mL/(g·h), 30 °C.	39%	65%	4
Pd/TiO ₂ -R	20 ppm HCHO, WHSV 200,000 mL/(g·h), 30 °C	93%	100%	4
Pd/TiO ₂ -H ₂	50 ppm HCHO, WHSV 24,000 mL/(g·h), 30 °C	100% (RH<5%)	100%	5
Pt/Beta-Si	80 ppm HCHO, O ₂ 20 vol% WHSV=60,000 mL/(g·h), 25 °C	80%	100% (RH=90%)	6
Pt/SBT-400	100 ppm HCHO, O ₂ 20 vol% WHSV=60,000 mL/(g·h), 25 °C	≈10%	≈50%	7
Rh/TiO ₂	140 ppm HCHO, O ₂ 20 vol% WHSV=30,000 mL/(g·h), 40 °C	≈15%	100% (RH≥50%)	8
Ir/TiO ₂	200 ppm HCHO, O ₂ 20 vol% GHSV=200,000 h ⁻¹ , 25 °C	0	30%	9
Na-Ir/TiO ₂	200 ppm HCHO, O ₂ 20 vol% GHSV=200,000 h ⁻¹ , 25 °C	0	80%	9
Pd/TiO ₂ -450R	300 ppm HCHO, O ₂ 20 vol% GHSV=95,000 h ⁻¹ , 25 °C	20%	80%	10
Pt/TiNB-ac	400 ppm HCHO, O ₂ 20 vol% GHSV=95,000 h ⁻¹ , 25 °C, WHSV=60,000 mL/(g·h), 20 °C	70%	90%	11
Pt/TiO ₂ (A)R	24 ppm HCHO, O ₂ 20 vol% GHSV=60,000 h ⁻¹ , 25 °C	99%	100%	12
Pt/TiO ₂ (B)R	24 ppm HCHO, O ₂ 20 vol% GHSV=60,000 h ⁻¹ , 25 °C	10%	100%	12
Pd/SiO₂	150 ppm HCHO, O₂ 20 vol% WHSV=600,000	50.5%	0	This work

mL/(g·h), 25 °C				
Na-Pd/SiO₂	150 ppm HCHO, O₂ 20	vol% WHSV=600,000	100%	0
	mL/(g·h), 25 °C			This work

Table S2. Specific surface area (BET) of SiO₂, Na/SiO₂, Pd/SiO₂ and Na-Pd/SiO₂ catalysts, and Pd dispersion (D_{co}), Pd average particle size (*d*_M) and TOF on Pd/SiO₂ and Na-Pd/SiO₂ catalysts

Samples	S _{BET} (m ³ /g)	D _{co} ^a (%)	TOF×10 ⁻² ^b (s ⁻¹)	<i>d</i> _M (nm)
SiO ₂	210.6	-	-	-
Na/SiO ₂	176.5	-	-	-
Pd/SiO ₂	152.5	1.6	1.3	9.85
Na-Pd/SiO ₂	143.8	21.0	4.0	4.87

^a Pd dispersion measured with CO pulse chemisorption.

^b Turnover frequencies (TOF) calculated from D_{co}.

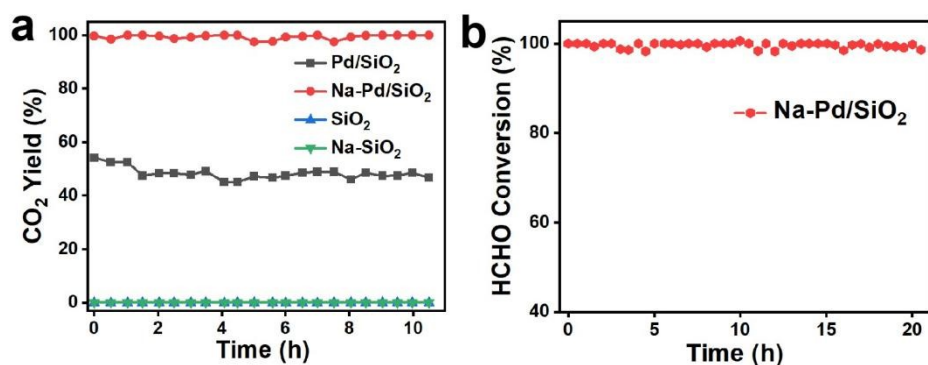


Fig. S1. CO₂ yield rate over SiO₂, Na/SiO₂, Pd/SiO₂, Na-Pd/SiO₂ samples (a), long-time test over Na-Pd/SiO₂ catalyst (b). Reaction conditions: 25 °C, 150 ppm of HCHO, 20% O₂, He balance, and WHSV = 600,000 mL / (g h).

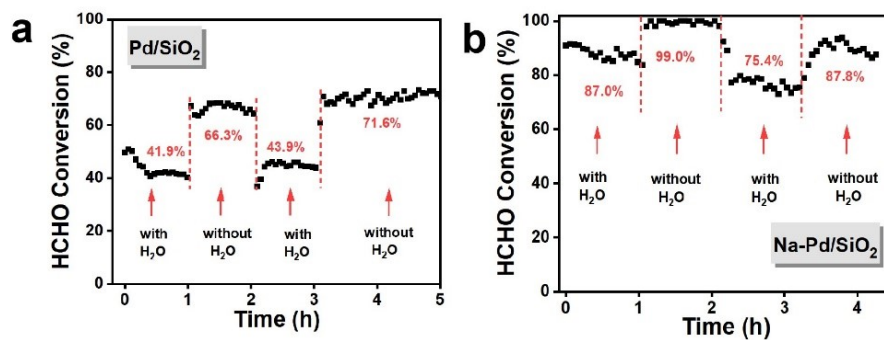


Fig. S2. Turn on and off the water experiment on Pd/SiO₂ and Na-Pd/SiO₂ catalysts.

Reaction conditions: 25 °C, 150 ppm of HCHO, 20% O₂, (35% RH or 0), He balance,

and WHSV = 600,000 mL / (g h).

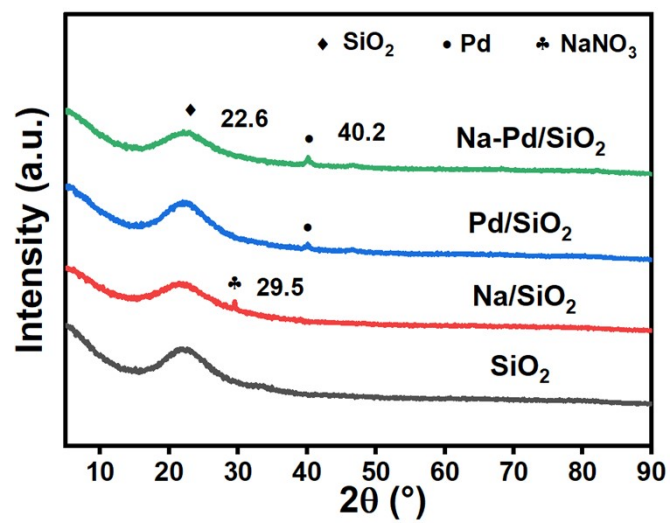


Fig. S3. XRD patterns of SiO₂, Na/SiO₂, Pd/SiO₂ and Na-Pd/SiO₂ samples.

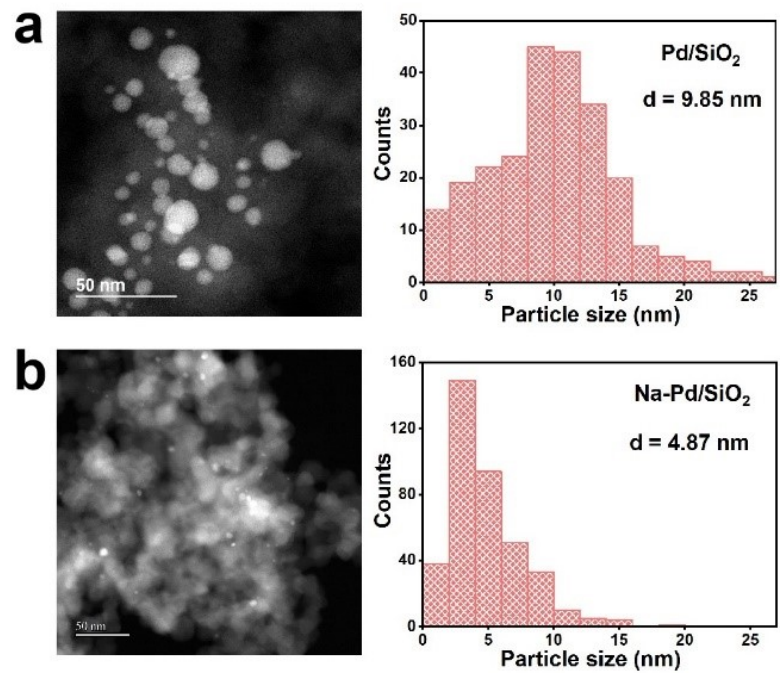


Fig. S4. STEM images and particle size distribution of Pd/SiO₂ (a), Na-Pd/SiO₂ (b) samples.

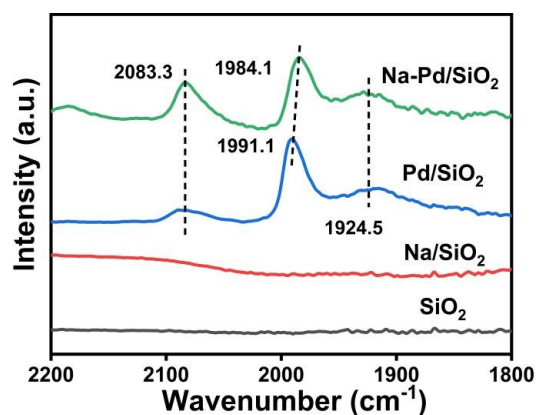


Fig. S5. CO *in situ* DRIFTS adsorption spectra on the SiO₂, Na/SiO₂, Pd/SiO₂, Na-Pd/SiO₂ catalysts.

Thanks for your question. The test of *in situ* DRIFTS adsorption of CO was added and displayed in Fig. S5. There were no CO adsorption peaks observed on the SiO₂ and Na/SiO₂ samples, which means the adsorption of CO is mainly related to precious metals. For Pd/SiO₂ and Na-Pd/SiO₂ catalysts, three CO adsorption peaks, at 2083.3, 1991.1-1984.1 and 1924.5 cm⁻¹, were observed and which were ascribed to linear adsorption, bridge adsorption at step site and bridge adsorption at terrace site^{13, 14}. Obviously, there were more linear adsorption on the Na-Pd/SiO₂ catalyst, indicating that the precious metal particles are smaller. The result was consistent with TEM conclusions.

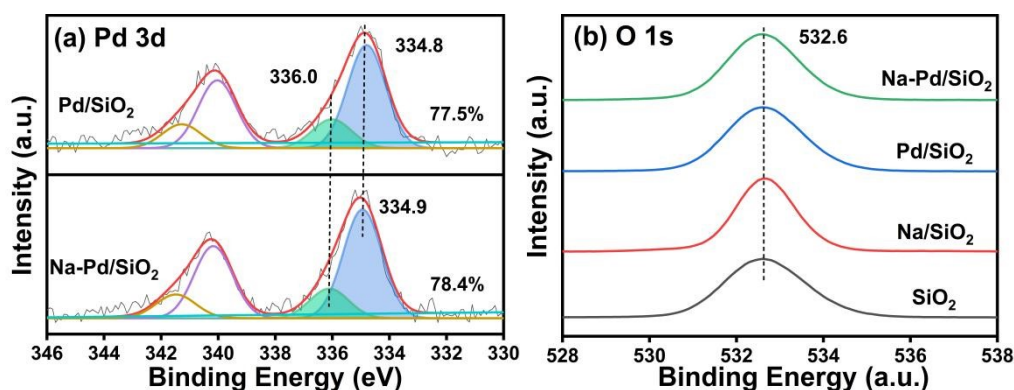


Fig. S6. XPS spectra of Pd 3d (a), O 1s (b) on the SiO₂, Na/SiO₂, Pd/SiO₂, Na-Pd/SiO₂ catalysts.

The XPS spectra of Pd and O elements were tested and displayed in Fig. S6. From Fig. S6 (a), two Pd species were observed on the Pd/SiO₂ and Na-Pd/SiO₂ catalysts. The peaks at 336.0 eV were assigned to Pd²⁺ species, while the peaks at 334.8 or 334.9 eV were ascribed to metallic Pd species², and the proportion of metallic Pd groups on the Pd/SiO₂ and Na-Pd/SiO₂ catalysts were 77.5% and 78.4% respectively. The results indicated that the Pd groups were similar on the two catalysts. From Fig. S6 (b), there were only one peak observed on the four samples. The peak at 532.6 eV was ascribed to lattice oxygen of SiO₂ bulk phase¹⁵. XPS tests demonstrated Pd and O species are similar on the two catalysts.

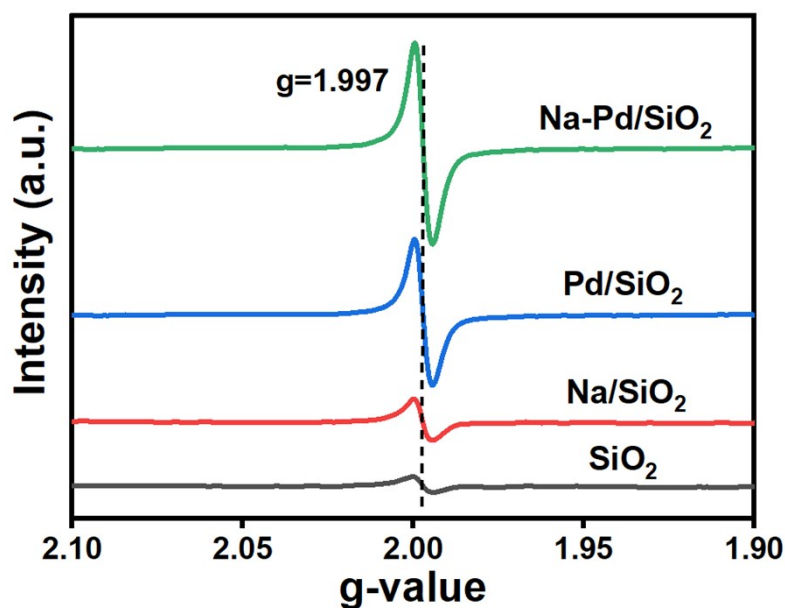


Fig. S7. ESR profiles of SiO_2 , Na/SiO_2 , Pd/SiO_2 and Na-Pd/SiO_2 catalysts.

Low temperature electron spin resonance (ESR) was then employed here to reveal the oxygen vacancy properties in the samples. The ESR spectra in Fig. S7 show that all of the four catalysts displayed a signal at $g = 1.997$, corresponding to typical signal from oxygen vacancy. More importantly, the signal intensity of oxygen vacancy increases along with the order of $\text{Na-Pd/SiO}_2 > \text{Pd/SiO}_2 > \text{Na/SiO}_2 \approx \text{SiO}_2$. Surface oxygen consumption by overflow hydrogen species during catalyst reduction, so catalysts with higher Pd dispersion and more hydrogen overflow sites possessed more oxygen vacancies. The result of ESR was in line with the distribution test data of Pd species.

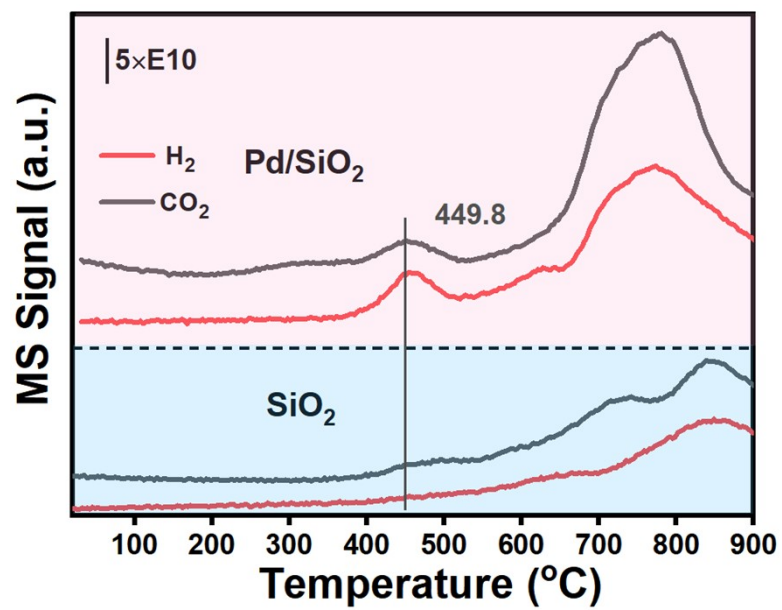


Fig. S8. CO-TPR profiles of SiO₂ and Pd/SiO₂ samples.

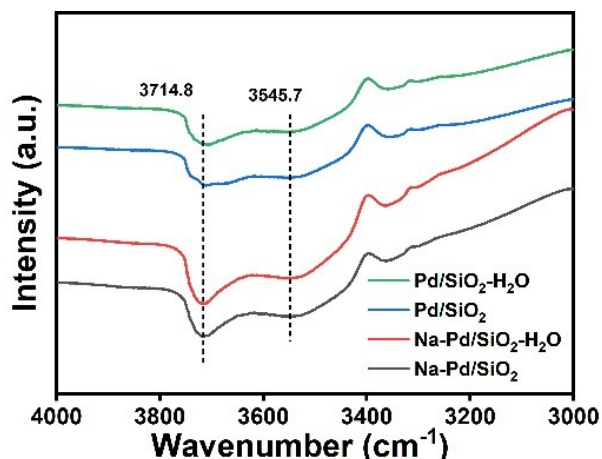


Fig. S9. NH_3 *in situ* DRIFTS adsorption spectra on Pd/SiO_2 , $\text{Pd}/\text{SiO}_2\text{-H}_2\text{O}$, $\text{Na-Pd}/\text{SiO}_2$ and $\text{Na-Pd}/\text{SiO}_2\text{-H}_2\text{O}$ samples. (The catalysts pretreated by RH 35% H_2O at 25 °C for 30 min were marked as $\text{Pd}/\text{SiO}_2\text{-H}_2\text{O}$ and $\text{Na-Pd}/\text{SiO}_2\text{-H}_2\text{O}$ catalysts)

The NH_3 *in situ* DRIFTS adsorption test at 25 °C was carried out to investigate the ability of catalysts to active water at room temperature. From Fig. S9, the NH_3 consumption peaks at 3714.8 and 3545.7 cm^{-1} were ascribed to terminal OH and silanol nests, respectively¹⁶. There were more OH groups on the catalysts after Na addition. However, compared to Pd/SiO_2 and $\text{Na-Pd}/\text{SiO}_2$ catalysts, the content of OH on the catalysts pretreated by H_2O were similar, which also proved that the Pd/SiO_2 and $\text{Na-Pd}/\text{SiO}_2$ catalysts have little ability to active water.

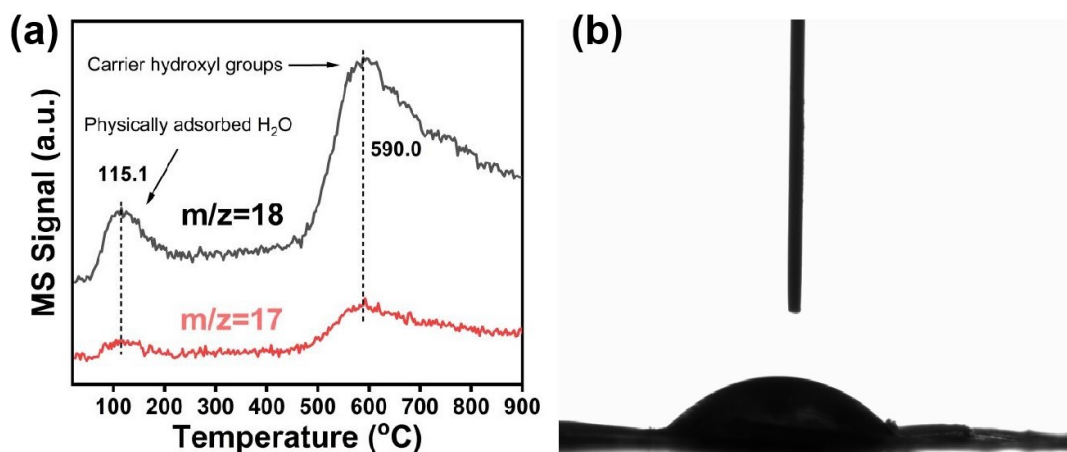


Fig. S10. H₂O-TPD (a) and contact angle (b) tests of SiO₂ carriers.

H₂O-TPD and contact angle tests were performed to explore the hydrophilicity of the SiO₂ carrier. From Fig. S10a, H₂O-TPD result shows that there are two H₂O desorption peaks on SiO₂ samples, respectively at 115.1 and 590.0 °C, which are attributed to the physical adsorption of water and the bulk phase hydroxyl group on the catalyst surface, respectively. From Fig. S10b, when a water droplet was brought into contact with the surface of SiO₂ carrier, it delivered a contact angle of 37.4°, indicating the hydrophilic nature of the support¹⁷. The vector of SiO₂ support was hydrophilic by combining both the characteristics.

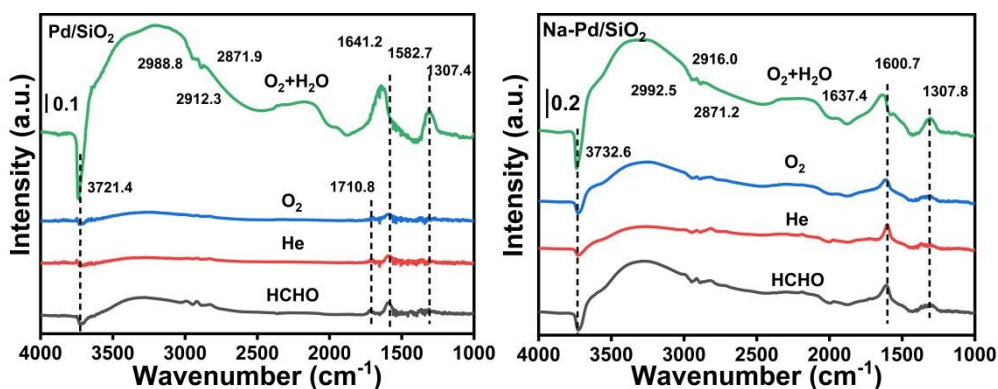
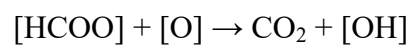
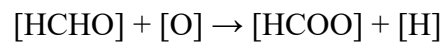


Fig. S11. The *in situ* DRIFT_S spectra over Pd/SiO₂ and Na-Pd/SiO₂ in a flow of HCHO for 30 min (1); followed by He purging for 30 min (2); and by O₂ + He purging for 30 min (3); finally, by O₂ + H₂O + He purging for 30 min at room temperature (4). Reaction conditions: 150 ppm of HCHO, 20% O₂, 35% RH, He balance, total flow rate of 100 mL / min.

Thanks for your question. The reaction mechanisms of HCHO oxidation on Pd/SiO₂ and Na-Pd/SiO₂ catalysts at room temperature were supplemented by *in situ* DRIFT_S test. The spectra of the catalysts at steady state under different gas flows are shown in Fig. S11. Firstly, the catalyst was exposed to a flow of HCHO + He for 30 min. With the consumption of surface hydroxyl species (3721.4-3732.6 cm⁻¹ for ν (OH)), formate species (1596 cm⁻¹ for ν (COO) and 2871.2, 2916.0 and 2992.5 cm⁻¹ for ν (C-H)) appeared². Differently, on Pd/SiO₂ catalysts, HCHO species was observed (1710.8 cm⁻¹)¹⁸, which means there were fewer reactive oxygen species on the surface of Pd/SiO₂ catalyst. After HCHO adsorption saturation, the system was purged by He for 30 min and the bands of formate and HCHO were decreased slightly. When oxygen was introduced into the system, formate and HCHO species further decrease. This indicates that oxygen species are beneficial to formate degradation. Finally, water and oxygen were introduced into the system, hydroxyl groups (3400.0 and 1637.4 cm⁻¹) appeared, meanwhile a band at 1307.8 cm⁻¹ associated with water was also appeared. The experimental results showed that the intermediate products did not decrease with the addition of water, which was in consistent with the experimental results of catalyst activity. Differently from previous studies¹⁹, hydroxyl groups are not involved in the catalytic reaction. Degradation mechanism of HCHO over Pd/SiO₂ and Na-Pd/SiO₂

catalysts maybe followed the reaction paths:



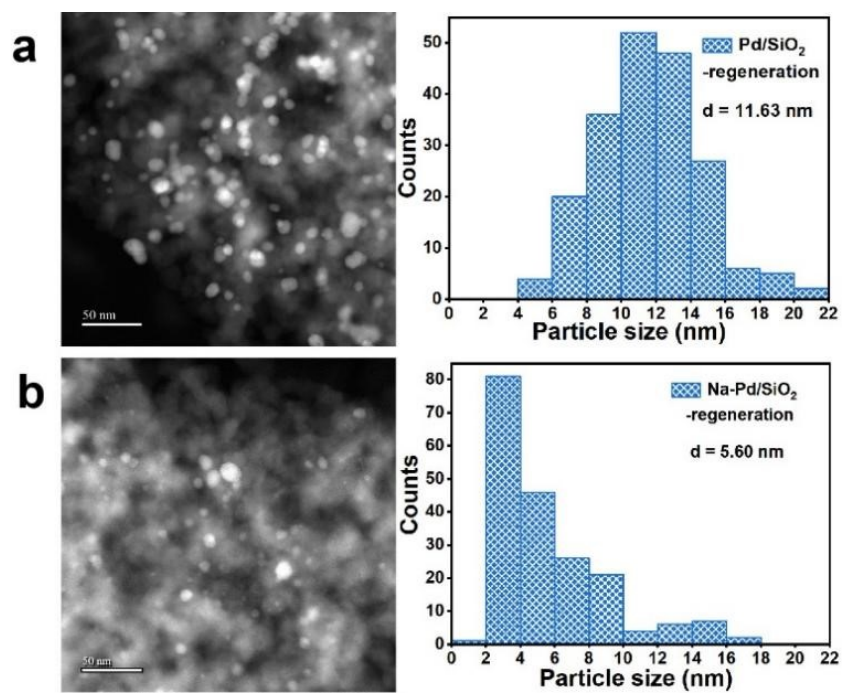


Fig. S12. STEM images and particle size distribution of regenerated samples

(Pd/SiO₂-regeneration (a), Na-Pd/SiO₂-regeneration (b)).

References

1. C. Wang, Y. Li, L. Zheng, C. Zhang, Y. Wang, W. Shan, F. Liu, H. He, A Nonoxide Catalyst System Study: Alkali Metal-Promoted Pt/AC Catalyst for Formaldehyde Oxidation at Ambient Temperature, *ACS Catal.*, 2020, **11**, 456-465.
2. C. Wang, Y. Li, C. Zhang, X. Chen, C. Liu, W. Weng, W. Shan, H. He, A simple strategy to improve Pd dispersion and enhance Pd/TiO₂ catalytic activity for formaldehyde oxidation: The roles of surface defects, *Appl. Catal. B*, 2021, **282**, 119540-119547.
3. C. Zhang, Y. Li, Y. Wang, H. He, Sodium-Promoted Pd/TiO₂ for Catalytic Oxidation of Formaldehyde at Ambient Temperature, *Environ. Sci. Technol.*, 2014, **48**, 5816-5822.
4. M. He, Y. Cao, J. Ji, K. Li, H. Huang, Superior catalytic performance of Pd-loaded oxygen-vacancy-rich TiO₂ for formaldehyde oxidation at room temperature, *J Catal.*, 2021, **396**, 122-135.
5. X. Wang, X. Zou, Z. Rui, Y. Wang, H. Ji, Highly dispersed and active Pd nanoparticles over titania support through engineering oxygen vacancies and their anchoring effect, *AIChE J*, 2020, **66**, 16288-16299.
6. L. Zhang, Y. Jiang, B. Chen, C. Shi, Y. Li, C. Wang, S. Han, S. Pan, L. Wang, X. Meng, F. Xiao, Exceptional activity for formaldehyde combustion using siliceous Beta zeolite as a catalyst support, *Catal. Today*, 2020, **339**, 174-180.
7. M. Huang, Y. Li, M. Li, J. Zhao, Y. Zhu, C. Wang, V. Sharma, Active Site-Directed Tandem Catalysis on Single Platinum Nanoparticles for Efficient and

- Stable Oxidation of Formaldehyde at Room Temperature, *Environ. Sci. Technol.*, 2019, **53**, 3610-3619.
8. X. Sun, J. Lin, H. Guan, L. Li, L. Sun, Y. Wang, S. Miao, Y. Su, X. Wang, Complete oxidation of formaldehyde over TiO₂ supported subnanometer Rh catalyst at ambient temperature, *Appl. Catal. B*, 2018, **226**, 575-584.
 9. Y. Li, X. Chen, C. Wang, C. Zhang, H. He, Sodium Enhances Ir/TiO₂ Activity for Catalytic Oxidation of Formaldehyde at Ambient Temperature, *ACS Catal.*, 2018, **8**, 11377-11385.
 10. Y. Li, C. Zhang, J. Ma, M. Chen, H. Deng, H. He, High temperature reduction dramatically promotes Pd/TiO₂ catalyst for ambient formaldehyde oxidation, *Appl. Catal. B*, 2017, **217**, 560-569.
 11. W. Cui, D. Xue, X. Yuan, B. Zheng, M. Jia, Jun, W. Zhang, Acid-treated TiO₂ nanobelt supported platinum nanoparticles for the catalytic oxidation of formaldehyde at ambient conditions, *Appl. Surf. Sci.*, 2017, **411**, 105-112.
 12. D. Kwon, P. Seo, G. Kim, S. Hong, Characteristics of the HCHO oxidation reaction over Pt/TiO₂ catalysts at room temperature: The effect of relative humidity on catalytic activity, *Appl. Catal. B*, 2015, **163**, 436-443.
 13. J. Chen, J. Zhong, Y. Wu, W. Hu, P. Qu, X. Xiao, G. Zhang, X. Liu, Y. Jiao, L. Zhong, Y. Chen, Particle Size Effects in Stoichiometric Methane Combustion: Structure-Activity Relationship of Pd Catalyst Supported on Gamma-Alumina. *ACS Catal.* 2020, **10**, (18), 10339-10349.

14. E. J. Jang, J. Lee, D. G. Oh, J. H. Kwak, CH₄ Oxidation Activity in Pd and Pt-Pd Bimetallic Catalysts: Correlation with Surface PdO_x Quantified from the DRIFTS Study. *ACS Catal.*, 2021, **11**, (10), 5894-5905.
15. S. Chen, S. Gueddida, M. Badawi, S. Lebègue, J.-M. Giraudon, J. Dhainaut, S. Royer, J.-F. Lamonier, Unravelling the critical role of silanol in Pt/SiO₂ for room temperature HCHO oxidation: An experimental and DFT study. *Appl. Catal. B*, 2023, **331**, 122672-122684.
16. G. Hou, T. Fu, X. Li, Q. Ma, Z. Li, Creation of silanol nests on HZSM-5 catalyst to boost the alkylation of toluene with methanol for PX synthesis. *Appl. Catal. A*, 2022, **642**, 118713-118725.
17. J. Lin, T. Wang, J. Zhou, X. Wu, Z. Ma, S. Liu, Elucidating water's place in catalytic C₃H₆ combustion over Pt@TiO_x/TiO₂ with super-hydrophilic silica-modified surface. *Appl. Catal. B*, 2023, **324**, 122234-122243.
18. X. Liu,; C. Wang,; Y. Li,; H. He,, Acid pretreatment of support promotes Pd/SiO₂ activity for formaldehyde oxidation at room temperature. *Catal. Sci. Technol.*, 2022, **12**, (21), 6540-6547.
19. J. Guo, C. Lin, C. Jiang, P. Zhang, Review on noble metal-based catalysts for formaldehyde oxidation at room temperature. *Appl. Surf. Sci.*, 2019, **475**, 237-255.